Crystal structure of racemic afoxolaner, C₂₆H₁₇CIF₉N₃O₃

James Kaduk^{1,2}, Anja Dosen³ and Tom Blanton³

¹Illinois Institute of Technology, Department of Chemistry, Chicago, IL, USA

(Received 16 May 2025; revised 24 July 2025; accepted 20 August 2025)

Abstract: The crystal structure of racemic afoxolaner has been solved and refined using synchrotron X-ray powder diffraction data and optimized using density functional theory techniques. Afoxolaner crystallizes in space group $P2_1/a$ (#14) with a = 9.6014(6), b = 14.0100(11), c = 39.477(10) Å, $\beta = 94.389$ (7)°, V = 5,294.7(17) ų, and Z = 8 at 298 K. The crystal structure consists of layers of molecules parallel to the ab-plane. The boundaries of the layers are rich in halogens. Within the layers, there is parallel stacking of rings along both the a- and b-axes. Two classical N–H···O hydrogen bonds link the two independent molecules into dimers. The powder pattern has been submitted to the International Centre for Diffraction Data (ICDD®) for inclusion in the Powder Diffraction FileTM (PDF®).

© The Author(s), 2025. Published by Cambridge University Press on behalf of International Centre for Diffraction Data. This is an Open Access article, distributed under the terms of the Creative Commons Attribution licence (http://creativecommons.org/licenses/by/4.0), which permits unrestricted re-use, distribution and reproduction, provided the original article is properly cited. [doi:10.1017/S0885715625101048]

Key words: afoxolaner, NEXGARD®, crystal structure, Rietveld refinement, density functional theory

I. INTRODUCTION

Afoxolaner is an insecticide and is the active ingredient in veterinary products, including NexGard[®]. Afoxolaner is used for the treatment and prevention of flea infestations, as well as Lyme disease, particularly for dogs. The systematic name (CAS Registry Number 1093861-60-9) is 4-[5-[3-chloro-5-(trifluoromethyl)phenyl]-4,5-dihydro-5-(trifluoromethyl)-3-isoxazolyl]-N-[2-oxo-2-[(2,2,2-trifluoroethyl)amino]ethyl]-1-naphth alenecarboxamide. A two-dimensional molecular diagram of afoxolaner is shown in Figure 1.

Crystalline Form I and Form II, and the corresponding powder diffraction data, of (S)-afoxolaner are claimed in U.S. Patent Application 2018/0354917 A1 (Gorter de Vries et al., 2018; Merial Inc.) and the issued patent US 11130739 B2 (Gorter de Vries et al., 2021; Boehringer Ingelheim Animal Health USA, Inc.). A synchrotron powder diffraction, from this study, of commercial afoxolaner did not correspond to those of Form I or Form II (Figure 2).

This work was carried out as part of a project (Kaduk et al., 2014) to determine the crystal structures of large-volume commercial pharmaceuticals and include high-quality powder diffraction data for them in the Powder Diffraction File (Kabekkodu et al., 2024).

II. EXPERIMENTAL

Afoxolaner was a commercial reagent, purchased from TargetMol (Batch #T13536), and was used as received. The

Corresponding author: James Kaduk; Email: kaduk@polycrystallography.

white powder was packed into a 0.5-mm-diameter Kapton capillary and rotated during the measurement at ~2 Hz. The powder pattern was measured at 298(1) K at the Wiggler Low Energy Beamline (Leontowich et al., 2021) of the Brockhouse X-ray Diffraction and Scattering Sector of the Canadian Light Source using a wavelength of 0.819563(2) Å (15.1 keV) from 1.6 to 75.0° 2θ, with a step size of 0.0025° and a collection time of 3 minutes. The high-resolution powder diffraction data were collected using eight Dectris Mythen2 X series 1K linear strip detectors. NIST SRM 660b LaB₆ was used to calibrate the instrument and refine the monochromatic wavelength used in the experiment. The peak/background ratio of this pattern is relatively low, resulting from low peak intensities.

The pattern was indexed using DICVOL14 (Louër and Boultif, 2014) on a primitive monoclinic unit cell with a = 9.6062, b = 14.0252, c = 39.3961 Å, $\beta = 94.782^{\circ}$, V = 5,289.32 Å³, and Z = 8. The space group suggested by EXPO2014 (Altomare et al., 2013) was $P2_1/a$, which was confirmed by the successful solution and refinement of the structure. A reduced cell search of the Cambridge Structural Database (Groom et al., 2016) yielded four hits, but no structures of afoxolaner or its derivatives. The centrosymmetric space group indicated that our sample was a racemate, consistent with the pattern not matching the known forms of (S)-afoxolaner.

The structure of the afoxolaner molecule was downloaded from PubChem (Kim et al., 2023) as Conformer3D_COMPOUND_CID_25154249.sdf. It was converted to a *.mol2 file using Mercury (Macrae et al., 2020). The structure was solved by Monte Carlo-simulated annealing techniques as implemented in EXPO2014 (Altomare et al., 2013),

²North Central College, Department of Physics, Naperville IL, USA

³International Centre for Diffraction Data (ICDD), Newtown Square, PA, USA

Figure 1. The two-dimensional structure of afoxolaner.

using two molecules as fragments and incorporating a bump penalty.

Rietveld refinement, starting from the VASP-optimized structure, was carried out with GSAS-II (Toby and Von Dreele, 2013). Only the $2.0-40.0^{\circ}$ portion of the pattern was included in the refinements ($d_{\min} = 1.198 \text{ Å}$). The region 2.6-3.4°, which contains a peak from the Kapton capillary, was excluded. All non-H-bond distances and angles were subjected to restraints, based on a Mercury/Mogul Geometry Check (Bruno et al., 2004; Sykes et al., 2011). The Mogul average and standard deviation for each quantity were used as the restraint parameters. The benzene and naphthalene ring systems were restrained to be planar. The restraints contributed 11.6% to the overall χ^2 . The hydrogen atoms were included in calculated positions, which were recalculated during the refinement using Materials Studio (Dassault Systèmes, 2023). Attempts to refine the displacement coefficients in such a complex structure with limited data led to unreasonable $U_{\rm iso}$ values (both positive and negative), so the $U_{\rm iso}$ values were fixed at reasonable values. The peak profiles were described using a generalized microstrain model (Stephens, 1999). A second-order spherical harmonic model was included for preferred orientation. The background was modeled using a six-term shifted Chebyshev polynomial,

with a peak at 11.26° to model the scattering from the Kapton capillary and any amorphous component of the sample.

The final refinement of 267 variables using 14,881 observations and 234 restraints yielded the residual $R_{\rm wp} = 0.04118$. The largest peak (1.04 Å from F64) and hole (1.77 Å from C24) in the difference Fourier map were 0.15(4) and -0.16 (4) $e\text{Å}^{-3}$, respectively. The final Rietveld plot is shown in Figure 3. The largest features in the normalized error plot are evenly distributed among shapes, intensities, and positions.

The crystal structure of afoxolaner was optimized (fixed experimental unit cell) with density functional theory techniques using VASP (Kresse and Furthmüller, 1996) through the MedeA graphical interface (Materials Design, 2024). The calculation was carried out on 32 cores of a 144-core (768 GB memory) HPE Superdome Flex 280 Linux server at North Central College. The calculation used the GGA-PBE functional, a plane wave cutoff energy of 400.0 eV, and a k-point spacing of 0.5 Å^{-1} , leading to a 1 × 1 × 2 mesh, and took ~23.2 days. Single-point density functional calculations (fixed experimental cell) and population analysis were carried out using CRYSTAL23 (Erba et al., 2023). The basis sets for the H, C, N, and O atoms in the calculation were those of Gatti et al. (1994), and those for F and Cl were those of Peintinger et al. (2013). The calculations were run on a 3.5 GHz PC using eight k-points and the B3LYP functional, and took \sim 11.6 hours.

III. RESULTS AND DISCUSSION

The commercial sample of afoxolaner studied here did not correspond to Form I or Form II of (S)-afoxolaner, as the commercial sample is a racemate. The difference may not be significant for many analytical applications, but it would be crucial for pharmaceutical uses. It is thus unclear how relevant this structure is for materials in actual use.

2

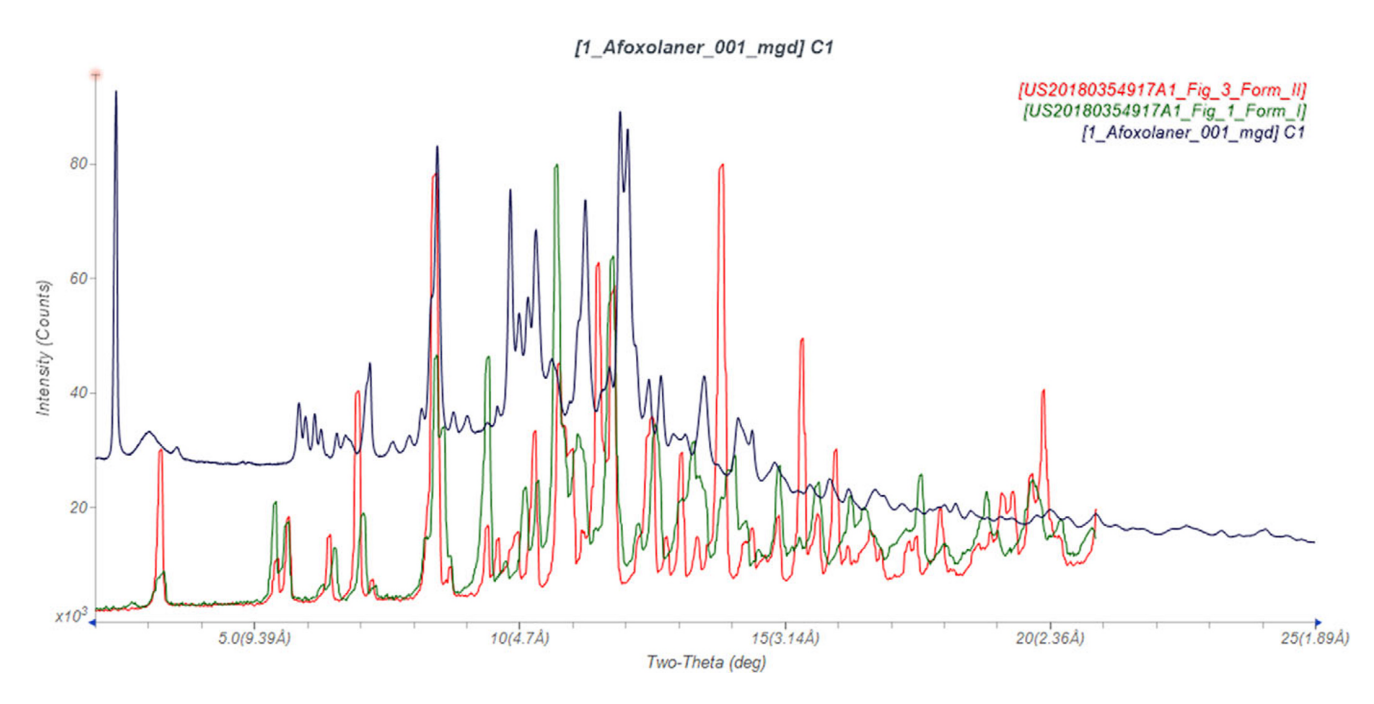


Figure 2. Comparison of the synchrotron pattern of afoxolaner (black) from this study to those of Form I (green) and Form II (red) reported by Gorter de Vries et al. (2018, 2021). The patent patterns (measured using Cu K_{α} radiation) were digitized using UN-SCAN-IT (Silk Scientific, 2013) and converted to the synchrotron wavelength of 0.819563(2) Å using JADE Pro (MDI, 2024). Image generated using JADE Pro (MDI, 2024).

Powder Diffr., 2025 Kaduk, Dosen and Blanton

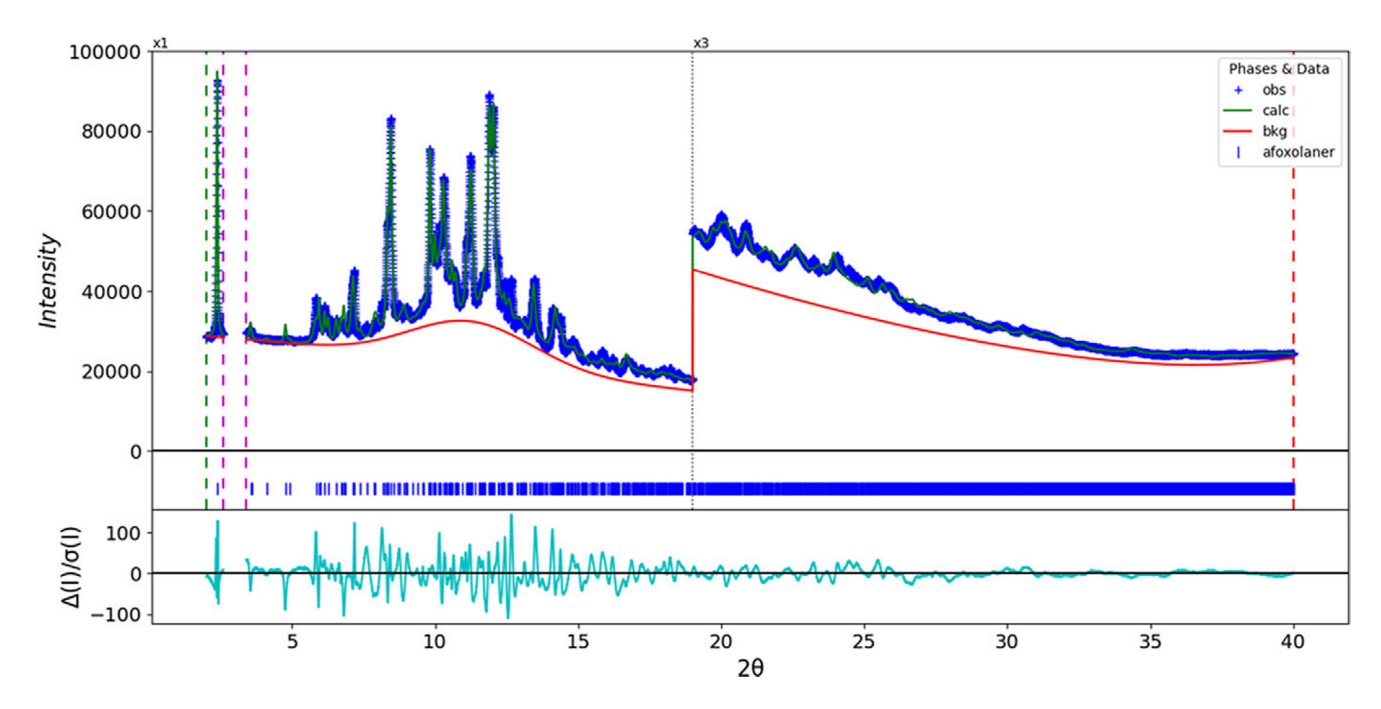


Figure 3. The Rietveld plot for afoxolaner. The blue crosses represent the observed data points, and the green line is the calculated pattern. The cyan curve is the normalized error plot, and the red line is the background curve. The vertical dashed magenta lines indicate the excluded region from 2.6 to 3.4. The blue tick marks indicate the afoxolaner peak positions. The vertical scale has been multiplied by a factor of $3 \times$ for $2\theta > 19.0$.

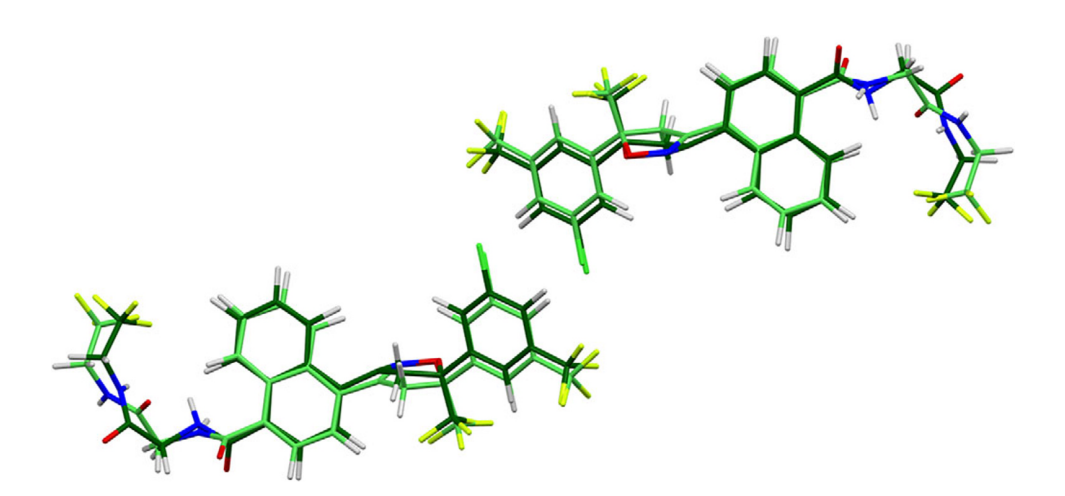


Figure 4. Comparison of the refined structure of afoxolaner (colored by atom type) to the VASP-optimized structure (light green). The comparison was generated by the Mercury CSD-Materials/Search/Crystal Packing Similarity tool; the root-mean-square displacement is 0.454 Å. Image generated using Mercury (Macrae et al., 2020).

The root-mean-square (rms) difference of the non-H atoms in the two optimized structures, calculated using the Mercury CSD-Materials/Search/Crystal Packing Similarity tool, is 0.454 Å (Figure 4). The main differences are in the conformations of the side chains. The rms Cartesian displacements of the non-H atoms in the optimized structures of molecule 1 and molecule 2, calculated using the Mercury Calculate/Molecule Overlay tool, are 0.799 and 0.583 Å (Figures 5 and 6). The main differences are in the side chains, but they are spread throughout the molecules. The agreements are outside the normal range for correct structures (van de Streek and Neumann, 2014). The broad peaks and limited data range probably mean that the refined structure is less reliable than usual. The refined structure has a close contact between

H27 and F64. The asymmetric unit is illustrated in Figure 7. The remaining discussion will emphasize the VASP-optimized structure.

All of the bond distances and bond angles, and most of the torsion angles, fall within the normal ranges indicated by a Mercury Mogul Geometry check (Macrae et al., 2020). Torsion angles involving rotation about the C17–C20, C39–C40, C78–C81, and C100–C101 bonds lie on the tails of distributions, so are slightly unusual. Torsion angles involving the C19–C22 bond, which describe the relative orientation of the isoxazole and naphthalene ring systems in molecule 1, are unusual. Torsion angles involving rotation about the C76–C79 bond, which describe the relative orientation of the phenyl and isoxazole rings in molecule 2, are also unusual.

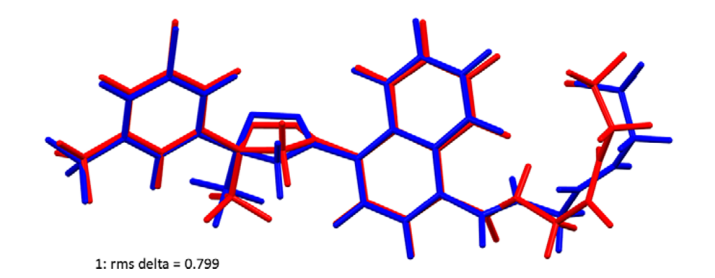


Figure 5. Comparison of the refined structure of afoxolaner molecule 1 (red) to the VASP-optimized structure (blue). The comparison was generated using the Mercury Calculate/Molecule Overlay tool; the root-mean-square difference is 0.799 Å. Image generated using Mercury (Macrae et al., 2020).

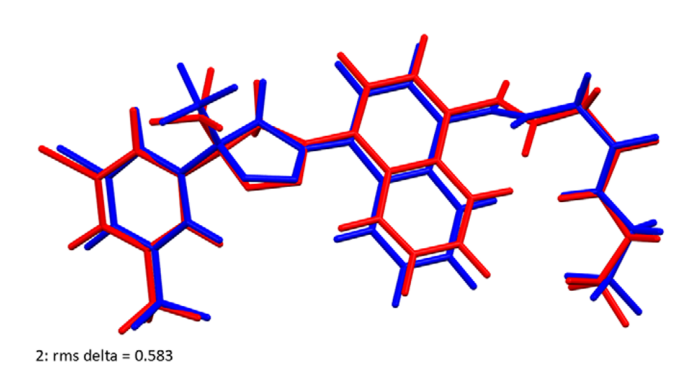


Figure 6. Comparison of the refined structure of afoxolaner molecule 2 (red) to the VASP-optimized structure (blue). The comparison was generated using the Mercury Calculate/Molecule Overlay tool; the root-mean-square difference is 0.583 Å. Image generated using Mercury (Macrae et al., 2020).

Quantum chemical geometry optimization of isolated afoxolaner molecules (DFT/B3LYP/6-31G*/water) using Spartan'24 (Wavefunction, 2023) indicated that molecule 1 is only 1.6 kcal/mol lower in energy than molecule 2, even though they have different conformations (Figure 8); the rms displacement is 2.166 Å. The global minimum-energy conformation is 3.9 kcal/mol lower in energy than molecule 1 and has a very different conformation. The afoxolaner molecule is thus apparently flexible, and intermolecular interactions are important in determining the solid-state conformation.



Figure 8. Comparison of molecule 1 (green) and molecule 2 (orange) of afoxolaner. The root-mean-square difference is 2.166 Å. Image generated using Mercury (Macrae et al., 2020).

The crystal structure (Figure 9) consists of layers of molecules parallel to the ab-plane. The boundaries of the layers are rich in halogens. Within the layers, there is parallel stacking of rings along both the a- and b-axes. The mean planes of the phenyl, isoxazole, and naphthalene rings in molecule 1 are approximately (-1, 0, -2), (0, 2, -1), and (-5, 5, 1), and in molecule 2, the planes are approximately (1, 0, -3). (0, 1, 0), and (-3, 3, -4). The Mercury Aromatics Analyser indicates a strong interaction (distance = 4.79 Å) between the naphthalene rings of molecules 1 and 2. Also present are moderate interactions between the phenyl rings of two molecules 1 (d = 5.17 Å) and between naphthalene rings (d = 4.98, 6.08, 6.28, and 6.39 Å).

The two classical N–H···O hydrogen bonds (Table I) link molecules 1 and 2 into dimers (Figure 10). The energies of the N–H···O hydrogen bonds were calculated using the correlation of Wheatley and Kaduk (2019). A variety of intra- and inter-molecular C–H···O, C–H···N, and C–H···C hydrogen bonds also contribute to the lattice energy. No C–H···F hydrogen bonds were detected.

The volume enclosed by the Hirshfeld surface of afoxolaner (Figure 11; Hirshfeld, 1977; Spackman et al., 2021) is 1,307.67 Å³, 98.79% of one-fourth of the unit cell volume. The packing density is thus typical. The only significant close contacts (red in Figure 11) involve the hydrogen bonds. The volume/non-hydrogen atom is slightly smaller than usual at 15.8 Å³.

The Bravais–Friedel–Donnay–Harker (Bravais, 1866; Friedel, 1907; Donnay and Harker, 1937) algorithm suggests

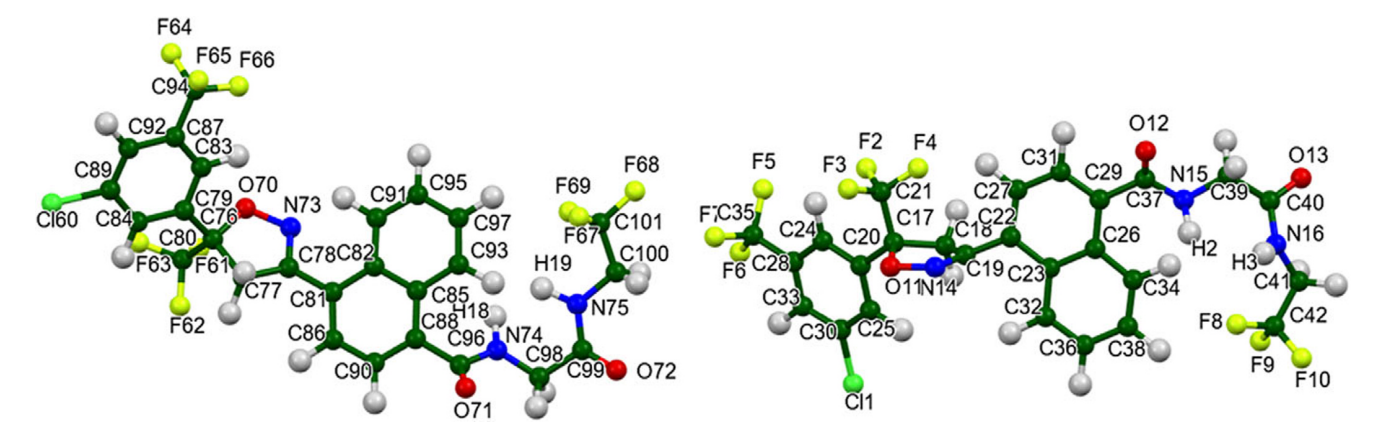


Figure 7. The asymmetric unit of afoxolaner, with the atom numbering. The atoms are represented by 50% probability spheroids. Image generated using Mercury (Macrae et al., 2020).

Powder Diffr., 2025 Kaduk, Dosen and Blanton

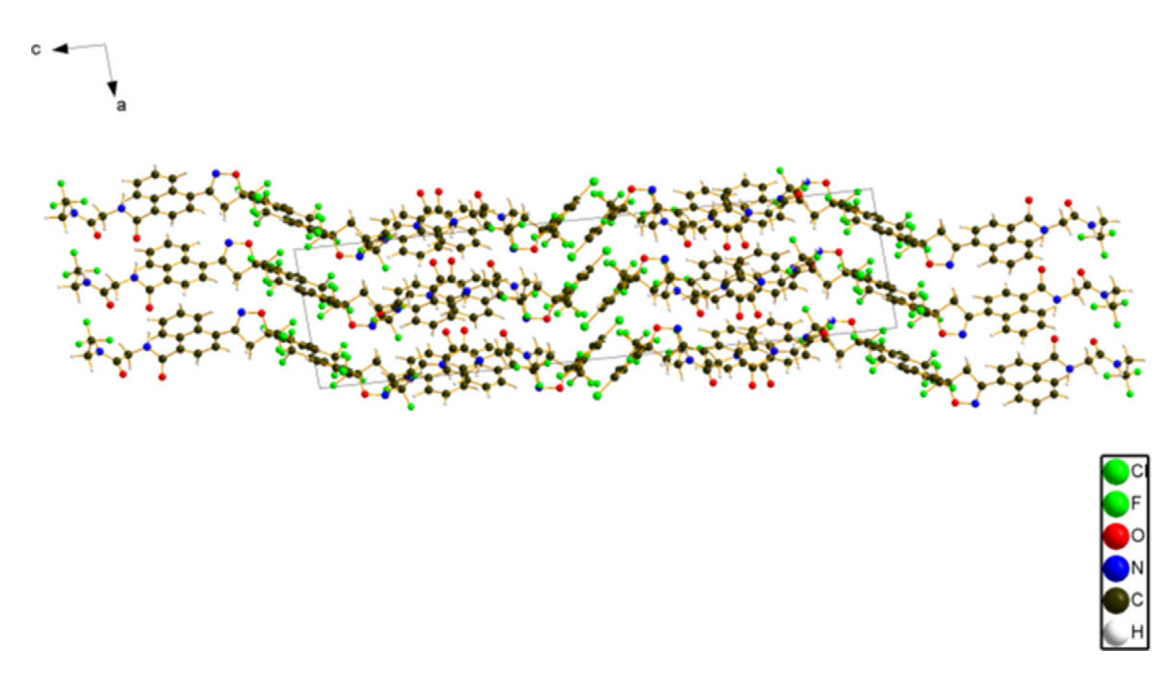


Figure 9. The crystal structure of afoxolaner, viewed down the b-axis. Image generated using Diamond (Crystal Impact, 2023).

TABLE I. Hydrogen bonds (CRYSTAL23) in racemic afoxolaner.

H bond	D–H, Å	H···A, Å	D···A, Å	D–H···A, °	Mulliken overlap, e	E, kcal/mol
N15-H2···O71	1.025	2.170	3.119	153.1	0.038	4.5
N74-H18···O12	1.026	2.424	3.372	153.2	0.028	3.9
C41-H58···O13	1.099	2.344*	2.774	101.1	0.019	
C18-H4···O72	1.098	2.713	3.774	162.5	0.012	
C25-H7···O72	1.090	2.477	3.492	154.5	0.018	
C39-H15···O12	1.098	2.490*	2.807	95.0	0.010	
C83-H22···O70	1.088	2.314*	2.710	98.7	0.011	
C97-H30···O71	1.091	2.655	3.429	127.4	0.010	
C98-H31···O71	1.103	2.414*	2.878	103.5	0.015	
C18-H5N14	1.100	2.533	3.463	141.6	0.017	
C91-H26···N73	1.090	2.293*	2.986	119.6	0.017	
C32-H10···C19	1.091	2.602*	2.961	98.2	0.011	
C93-H28···C96	1.090	2.491*	2.881	99.6	0.013	
C98-H32···C32	1.096	2.438	3.464	155.4	0.012	

^{*}Intramolecular.

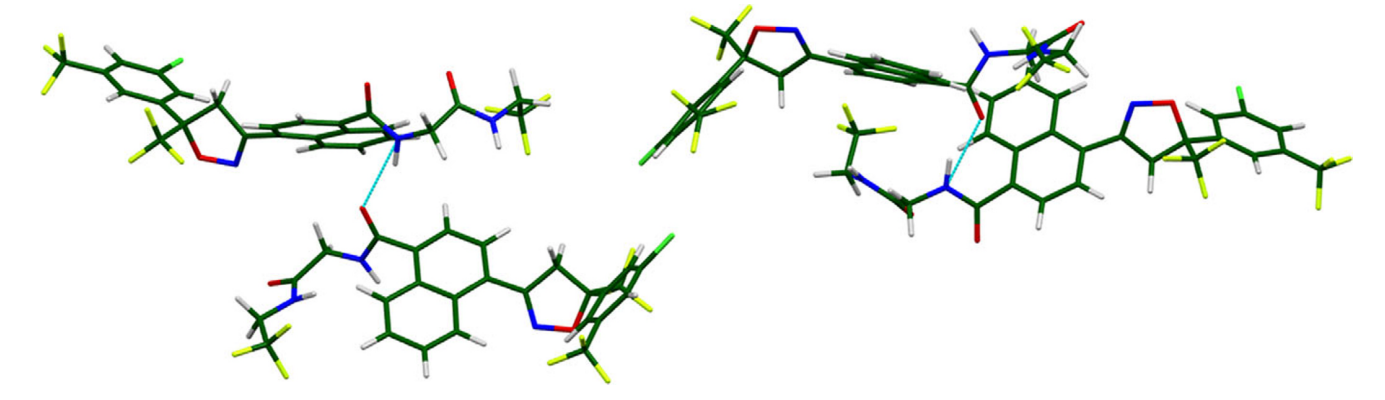


Figure 10. The two different hydrogen-bonded dimers in the structure of afoxolaner. The cyan dotted lines indicate the hydrogen bonds. Image generated using Mercury (Macrae et al., 2020).

that we might expect platy morphology for afoxolaner, with {001} as the major faces, as expected from the anisotropy of the lattice parameters. A second-order spherical harmonic

model was included in the refinement. The texture index was 1.062(36), indicating that the preferred orientation was significant in this rotated capillary specimen.

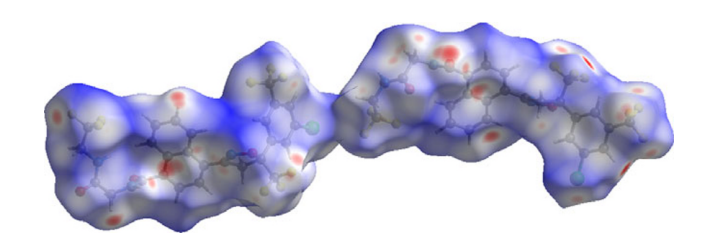


Figure 11. The Hirshfeld surface of afoxolaner. Intermolecular contacts longer than the sums of the van der Waals radii are colored blue, and contacts shorter than the sums of the radii are colored red. Contacts equal to the sums of radii are white. Image generated using CrystalExplorer (Spackman et al., 2021).

DEPOSITED DATA

The powder pattern of racemic afoxolaner from this synchrotron dataset has been submitted to the International Centre for Diffraction Data (ICDD) for inclusion in the Powder Diffraction File. The Crystallographic Information Framework (CIF) files containing the results of the Rietveld refinement (including the raw data) and the DFT geometry optimization were deposited with the ICDD. The data can be requested at pdj@icdd.com.

ACKNOWLEDGEMENTS

We thank Adam Leontowich for his assistance in the data collection. We also thank the ICDD team – Megan Rost, Steve Trimble, and Dave Bohnenberger – for their contribution to research, sample preparation, and in-house XRD data collection and verification.

FUNDING STATEMENT

Part of the research described in this paper was performed at the Canadian Light Source, a national research facility of the University of Saskatchewan, which is supported by the Canada Foundation for Innovation (CFI), the Natural Sciences and Engineering Research Council (NSERC), the Canadian Institute of Health Research (CIHR), the Government of Saskatchewan, and the University of Saskatchewan. This work was partially supported by the International Centre for Diffraction Data.

COMPETING INTERESTS

The authors have no competing interests to declare.

REFERENCES

- Altomare, A., C. Cuocci, C. Giacovazzo, A. Moliterni, R. Rizzi, N. Corriero, and A. Falcicchio. 2013. "EXPO2013: A Kit of Tools for Phasing Crystal Structures from Powder Data." *Journal of Applied Crystallography* 46: 1231–35
- Bravais, A. 1866. Etudes Cristallographiques. Paris: Gauthier Villars.
- Bruno, I. J., J. C. Cole, M. Kessler, J. Luo, W. D. S. Motherwell, L. H. Purkis, B. R. Smith, et al. 2004. "Retrieval of Crystallographically Derived Molecular Geometry Information." *Journal of Chemical Information* and Computer Sciences 44: 2133–44.
- Crystal Impact. 2023. *Diamond V. 5.0.0*. Bonn: Crystal Impact Dr. H. Putz & Dr. K. Brandenburg.

- Dassault Systèmes. 2023. BIOVIA Materials Studio 2024. San Diego, CA: BIOVIA.
- Donnay, J. D. H., and D. Harker. 1937. "A New Law of Crystal Morphology Extending the Law of Bravais." *American Mineralogist* 22: 446–67.
- Erba, A., J. K. Desmarais, S. Casassa, B. Civalleri, L. Donà, I. J. Bush, B. Searle, et al. 2023. "CRYSTAL23: A Program for Computational Solid State Physics and Chemistry." *Journal of Chemical Theory and Computation* 19: 6891–932. https://doi.org/10.1021/acs.jctc.2c00958.
- Friedel, G. 1907. "Etudes sur la loi de Bravais." Bulletin de la Société Française de Minéralogie 30: 326–455.
- Gatti, C., V. R. Saunders, and C. Roetti. 1994. "Crystal-Field Effects on the Topological Properties of the Electron-Density in Molecular Crystals – the Case of Urea." *Journal of Chemical Physics* 101: 10686–696.
- Gorter de Vries, R. J., B. Ballion, S. Lafont, M. G. de Saint Michel, and S. Kozlovic. 2018. "Crystalline Forms of (S)-Afoxolaner." U.S. Patent Application 2018/0354917.
- Gorter de Vries, R. J., B. Ballion, S. Lafont, M. G. de Saint Michel, and S. Kozlovic. 2021. "Crystalline Forms of (S)-Afoxolaner." U.S. Patent US 11130739 B2.
- Groom, C. R., I. J. Bruno, M. P. Lightfoot, and S. C. Ward. 2016. "The Cambridge Structural Database." Acta Crystallographica Section B: Structural Science, Crystal Engineering and Materials 72: 171–79.
- Hirshfeld, F. L. 1977. "Bonded-Atom Fragments for Describing Molecular Charge Densities." *Theoretica Chemica Acta* 44: 129–38.
- Kabekkodu, S., A. Dosen, and T. N. Blanton. 2024. "PDF-5⁺: A Comprehensive Powder Diffraction File[™] for Materials Characterization." *Powder Diffraction* 39: 47–59.
- Kaduk, J. A., C. E. Crowder, K. Zhong, T. G. Fawcett, and M. R. Suchomel. 2014. "Crystal Structure of Atomoxetine Hydrochloride (Strattera), C₁₇H₂₂NOCl." *Powder Diffraction* 29: 269–73.
- Kim S., J. Chen, T. Cheng, A. Gindulyte, J. He, S. He, Q. Li, et al. 2023. "PubChem 2023 Update." Nucleic Acids Research 51 (D1): D1373–80. https://doi.org/10.1093/nar/gkac956.
- Kresse, G., and J. Furthmüller. 1996. "Efficiency of Ab-Initio Total Energy Calculations for Metals and Semiconductors Using a Plane-Wave Basis Set." *Computational Materials Science* 6: 15–50.
- Leontowich, A. F. G., A. Gomez, B. Diaz Moreno, D. Muir, D. Spasyuk, G. King, J. W. Reid, C.-Y. Kim, and S. Kycia. 2021. "The Lower Energy Diffraction and Scattering Side-Bounce Beamline for Materials Science at the Canadian Light Source." *Journal of Synchrotron Radiation* 28: 1–9. https://doi.org/10.1107/S1600577521002496.
- Louër, D., and A. Boultif. 2014. "Some Further Considerations in Powder Diffraction Pattern Indexing with the Dichotomy Method." *Powder Diffraction* 29: S7–12.
- Macrae, C. F., I. Sovago, S. J. Cottrell, P. T. A. Galek, P. McCabe, E. Pidcock, M. Platings, et al. 2020. "Mercury 4.0: From Visualization to Design and Prediction." Journal of Applied Crystallography 53: 226–35.
- Materials Design. 2024. *MedeA 3.7.2*. San Diego, CA: Materials Design, Inc. MDI. 2024. *JADE Pro Version 9.0*. Livermore, CA: Materials Data.
- Peintinger, M. F., D. Vilela Oliveira, and T. Bredow. 2013. "Consistent Gaussian Basis Sets of Triple-Zeta Valence with Polarization Quality for Solid-State Calculations." *Journal of Computational Chemistry* 34: 451–59.
- Silk Scientific. 2013. UN-SCAN-IT 7.0. Orem, UT: Silk Scientific Corporation.
- Spackman, P. R., M. J. Turner, J. J. McKinnon, S. K. Wolff, D. J. Grimwood, D. Jayatilaka, and M. A. Spackman. 2021. "CrystalExplorer: A Program for Hirshfeld Surface Analysis, Visualization and Quantitative Analysis of Molecular Crystals." *Journal of Applied Crystallography* 54: 1006– 11. https://doi.org/10.1107/S1600576721002910; https://crystalexplorer.net.
- Stephens, P. W. 1999. "Phenomenological Model of Anisotropic Peak Broadening in Powder Diffraction." *Journal of Applied Crystallography* 32: 281–89
- Sykes, R. A., P. McCabe, F. H. Allen, G. M. Battle, I. J. Bruno, and P. A. Wood. 2011. "New Software for Statistical Analysis of Cambridge Structural Database Data." *Journal of Applied Crystallography* 44: 982–96.

Powder Diffr., 2025 Kaduk, Dosen and Blanton

- Toby, B. H., and R. B. Von Dreele. 2013. "GSAS II: The Genesis of a Modern Open Source All Purpose Crystallography Software Package." *Journal of Applied Crystallography* 46: 544–49.
- van de Streek, J., and M. A. Neumann. 2014. "Validation of Molecular Crystal Structures from Powder Diffraction Data with Dispersion-Corrected Density
- Functional Theory (DFT-D)." *Acta Crystallographica Section B: Structural Science, Crystal Engineering and Materials* 70: 1020–32.
- Wavefunction, Inc. 2023. Spartan'24. V. 1.0.0. Irvine, CA: Wavefunction, Inc. Wheatley, A. M., and J. A. Kaduk. 2019. "Crystal Structures of Ammonium Citrates." Powder Diffraction 34: 35–43.